

Quantum Monte Carlo study of MnO solid

Ji-Woo Lee

Department of Physics, Duke University, Durham, NC 27708-0305

Lubos Mitas and Lucas K. Wagner

Center for High Performance Simulation and Department of Physics,
North Carolina State University, Raleigh, NC 27695-8202

(dated: February 8, 2020)

Electronic structure of the manganese oxide solid is studied by the quantum Monte Carlo (QMC) methods. The trial wavefunctions are built using orbitals from unrestricted Hartree-Fock and Density Functional Theory, and the electron-electron correlation is recovered by the fixed-node QMC. The correlation effects are significant and QMC estimations of the gap and cohesion show a very good agreement with experiment. Comparison with hybrid functional results points out the importance of the exact exchange for improvement of the Density Functional description of transition metal oxide systems.

PACS numbers: 71.27.+a, 72.80.Ga, 71.20.-b, 71.15.Nc

Transition metal compounds and transition metal oxides (TMOs) in particular belong to the most complex and important types of solid materials. TMOs exhibit a multitude of collective effects such as ferro-, ferri- and anti-ferromagnetism, ferroelectricity, superconductivity, etc [1, 2]. The electronic structure of these systems poses a real challenge both for theory and experiment and TMOs have remained on a forefront of condensed matter research for decades [3, 4, 5, 6, 7, 8, 9, 10, 11]. Among the TMO solids, MnO and NiO have become paradigmatic examples of strong electron-electron correlation effects and antiferromagnetic ordering. Both MnO and NiO should nominally exhibit partially filled levels which would lead to a metallic ground state, however, experiments revealed that these systems are actually antiferromagnetic insulators with large gaps. The qualitative picture of electronic structure is explained either by a Mott-Hubbard mechanism implying that the gap results from a large local Coulomb repulsion in doubly occupied d-states, or by a charge transfer from transition metal d-states to oxygen p levels with the gap having p-d like character or a by a combined regime in between [3]. The localized d subshells exhibit unpaired spins which at low temperatures order into an antiferromagnetic AF II insulator with alternating spin (111) planes in cubic rocksalt structure.

The electronic structure of MnO and NiO have been studied by a number of theoretical approaches, most notably by the spin-polarized Density Functional Theory (DFT) with several types of functionals. Augmented spherical wave local density approximation calculations [5] and subsequent works [6] explained the stability of the AF II ordering in NiO and MnO. Very recently, the rhombohedral distortion of MnO was successfully described by accurate DFT calculations [4]. However, the commonly used DFT functionals are less reliable for predicting other key properties of strongly correlated sys-

tems. For example, DFT band gaps can be underestimated by a factor of 3-10 or even absent, leading thus to false metallic states. Therefore a variety of DFT modifications such as self-interaction correction [7, 8], orbital-polarization corrections [9], on-site Coulomb interaction (LDA+U approach) [10, 11] and others, have been suggested to improve the description of gaps and other electronic properties. On the other hand, Towler et al. [12] studied MnO and NiO with unrestricted Hartree-Fock theory (UHF). UHF is seemingly a poor method since it neglects the electron correlation completely. Nevertheless, for transition elements the exchange, which is exact in the HF theory, is at least as important as correlation, especially for metallic ions with an effective d subshells occupation close to half-filling. The UHF results confirmed the crucial role of exchange in TMOs and provided a complementary picture to DFT with overestimated gaps and underestimated cohesion, but also with the correct AF order, magnetic moments within 10% from experiments and reasonably accurate lattice constants. Moreover, unlike DFT approaches which predict insulator only for the AF II ground state, UHF keeps the gap open also for the ferromagnetic or any spin-disordered phases. This agrees with experiment which shows that MnO is an insulator well above the Neel temperature $T_N = 118\text{K}$ since the spin ordering Mn-O-Mn superexchange mechanism is very weak and hardly affected by spin flips on localized ions.

In this letter, we take a fresh look on the MnO system in the framework of many-body quantum Monte Carlo method (for example, Ref. [13] and references therein). Our aim is to understand and quantify the impact of explicit treatment of both exact exchange and correlation on the key properties such as cohesion and band gap. In spin systems the QMC method was very successful in capturing electron correlation effects for a large number of valence electrons [13]. It is therefore both important

and interesting to test the QMC performance on challenging problems such as TMOs, extending the previous attempts to apply QMC to NiO system [14, 15].

We employ variational Monte Carlo and the diffusion Monte Carlo (DMC) methods. The trial/variational wavefunction is expressed as a product of Slater determinants of single-particle spin-up and spin-down orbitals ($f' g; f' g$) multiplied by a Jastrow correlation factor [16, 17],

$$\Psi_T = D \prod_{f' g} \prod_{f' g} \exp \left[\sum_{I: i < j}^2 \sum_{I: i < j}^3 u(r_{iI}; r_{jI}; r_{ij}) \right]^5 ; \quad (1)$$

where I corresponds to the ions, i, j to the electrons and $r_{iI}; r_{jI}; r_{ij}$ to the distances. Similarly to the previous work [13, 14, 18] the correlation function consists of a linear combination of electron-electron and electron-ion terms and involves 9 variational parameters. The DMC method is used to remove the major part of variational bias which is inherent to the variational methods. DMC is based on the property that the projection $\lim_{\tau \rightarrow \infty} \exp(-H\tau)$ is proportional to the ground state for an arbitrary Ψ_T with the same symmetry and non-zero overlap [19]. The fermion sign problem caused by the antisymmetry of electrons is avoided by the commonly used fixed-node approximation.

In our calculations the core electrons are eliminated by pseudopotentials. For transition elements the choice of accurate pseudopotentials is far from trivial. In many TMO pseudopotential calculations with plane wave basis sets only the outermost d and s states are included into the valence space. However, earlier work [21] indicated that the errors from elimination of the so-called semicore states, such as $3s$ and $3p$ in the $3d$ transition series, could be significant. To elucidate this aspect, Table I. provides a comparison of the $s \rightarrow d$ excitation energies for the Mn atom as obtained by the DMC method using scalar relativistic large-core (Ar) [22] and small-core (Ne) pseudopotentials [23]. It is evident that inclusion of $3s$ and $3p$ states into the valence space is important. The large-core (Ar) pseudopotentials show errors of the order ~ 0.5 - 0.6 eV while the Ne-core pseudopotentials are much more accurate with typical errors ~ 0.1 eV, what is comparable to the bias from the fixed-node approximation [13]. The physical reason of such behavior is well-known and stems from the spatial distribution of the $3s, 3p$ electrons which is similar to the one of $3d$ electrons since they occupy the same principal shell. The price which one has to pay for using small core is, of course, significant. The magnitude of total energy, which is one of the key measures of QMC computational demands, increases roughly eightfold. It is also useful to notice that the DFT results for these excitations differ from experiments by 0.6 - 1 eV, clearly indicating the large contributions from exchange and correlation (Tab. I.).

TABLE I: The excitation energies [eV] $s \rightarrow d$ of the Mn atom as calculated by UHF, DFT (BLYP and B3LYP) and DMC methods. We used the Ne-core scalar relativistic pseudopotentials except for the DMC (Ar) calculations which employed the Ar-core pseudopotentials. In the last column are the experimental energies. Our DFT/BLYP results are close to similar calculations done previously, see Ref. [24].

	UHF	BLYP	B3LYP	DMC (Ar)	DMC (Ne)	Exp.
$s \rightarrow d$	3.5	1.2	1.6	1.6(1)	2.2(1)	2.1
$s^2 \rightarrow d^2$	9.1	4.4	5.2	5.2(1)	5.8(1)	5.6

For the MnO solid we first carried out calculations with the spin-unrestricted Hartree-Fock and DFT (B3LYP and PW86) methods and Ne-core pseudopotentials using the CRYSTAL98/03 packages [25]. The orbitals were expanded in gaussian basis sets with (12s;12p;7d) gaussians contracted to [3s;3p;2d] and (8s;8p;1d) contracted to [4s;4p;1d] for Mn and O atoms, respectively. Figure 1 shows the band structure of MnO solid which is obtained from UHF (a), B3LYP (b), PW86 (c) methods. Note that B3LYP hybrid functional contains 20% of the Hartree-Fock exchange so that it "interpolates" between the exact HF exchange and the effective local DFT exchange limits [26] and it often provides an improved picture of excitations both in molecules and solids.

In QMC the MnO solid is represented by a supercell with periodic boundary conditions. This way of simulating the actual solid involves finite size errors which scale as $1/N$ where N is the number of atoms in the supercell [28, 29]. The finite size errors affect mainly the estimation of cohesive energy where one needs to calculate the energy per primitive cell vs. isolated atoms. In order to filter out the finite size bias we have carried out VMC calculations of supercells with 8, 12, 16, 20 and 24 atom/supercell. The most accurate and extensive fixed-node DMC calculations were carried out with B3LYP orbitals for 16 and 20 atoms in the supercell. The cohesive energy obtained by the DMC method shows an excellent agreement with experiment (Tab. II). To evaluate the impact of the correlation on the gap we have estimated the energy of the $\rightarrow B$ excitation by an exciton calculation [18]. The QMC result for excitation energy is less perfect with the difference from experiment being a fraction of an eV. This clearly shows that the wavefunction and corresponding fixed-node error is larger for an excited state. Nevertheless, the differential energy gain for excited vs. ground state from correlation of ~ 8 eV is substantial and demonstrates the importance of this effect both in qualitative and quantitative sense. Due to large computational demands, similar but statistically less precise DMC calculations were carried out also with the UHF orbitals. While for the ground state the difference between the two sets of orbitals was marginal,

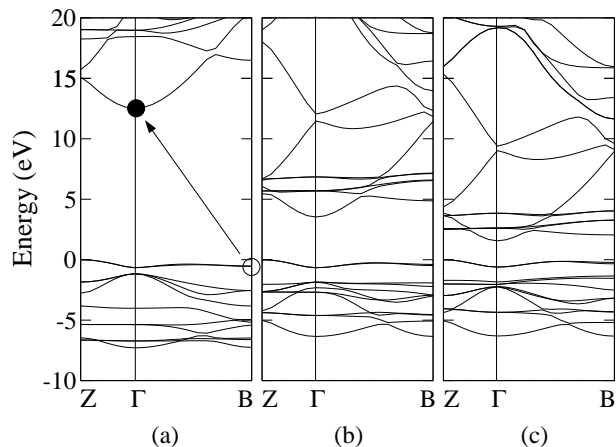


FIG. 1: The band structures of MnO obtained by (a) the unrestricted Hartree-Fock method, (b) DFT/B3LYP functional, and (c) DFT/PW86 functional. The PW91 and PBE functionals provide essentially the same picture as the PW86 functional. The calculated excitation in QMC is indicated by an arrow on the UHF plot and the corresponding one-particle states are denoted by open and filled circles.

the excited state with UHF orbitals appeared higher in energy approximately by 1.5(0.5) eV indicating thus, not surprisingly, even larger excited-state bias for the excited state in the UHF approach.

TABLE II: The MnO solid cohesive energy and B_{eff} excitation energy calculated by UHF, DFT and DMC methods compared with experiment. The determinantal part of the DMC wavefunction used the B3LYP one-particle orbitals.

	UHF	PW86	B3LYP	DMC	Exp.
E_{coh}	6.03	11.00	9.21	9.40 (5)	9.50
B_{eff}	13.5	1.2	4.0	4.8 (2)	4.1

It is quite encouraging that the excited-state DMC with the simplest possible single-determinant wavefunction leads to a consistent and parameter-free description of the basic properties of this strongly correlated system. An obvious question to ask is whether one-determinant is sufficiently accurate for an antiferromagnet since the wavefunction with different spin-up and spin-down orbitals is manifestly not an eigenfunction of the square of the total spin operator. In order to eliminate the spin contamination one would need to explore wavefunction forms beyond the single-determinant Slater-Jastrow, for example, generalized valence bond wavefunctions. However, since the actual mechanism is the Mn-O-Mn superexchange, one can expect the resulting effect to be small and most probably undetectable within our error bars (our calculations with wavefunctions beyond the single UHF determinant were not conclusive.)

It is interesting to revisit now the one-particle results and provide some feedback from our QMC calculations.

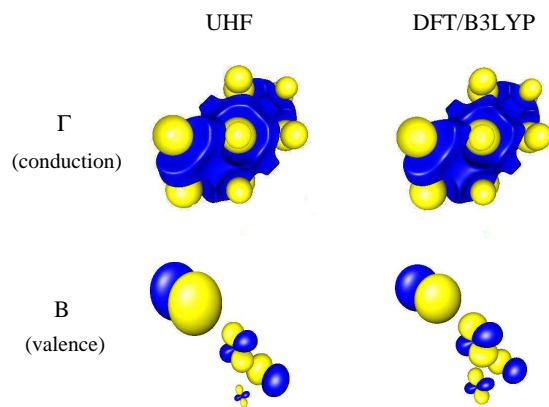


FIG. 2: Isosurfaces of UHF and DFT/B3LYP (blue/dark region is positive while yellow/light is negative). The valence B states are plotted for four atoms while the conduction states are plotted for a supercell so that their conducting character is visible. The valence states have significant weights both from Mn d states and O p states. Note small increase/decrease of d-p orbital amplitudes from UHF to DFT/B3LYP. The conduction state is much more delocalized and is composed from Mn 4s and O 3s atomic states.

The analysis of orbitals indicates that the nature of the top valence bands is rather similar in all approaches with both p and d states having significant weights in these states across the Brillouin zone (see Fig. 2). This is clear also from the Mulliken population analysis which shows effective magnetic moments on Mn atoms in UHF, B3LYP and PW86/PW91/PBE methods to be 4.92, 4.84 and 4.78 μ_B , respectively; these values are quite close to each other and border the range of experimental estimates of 4.58-4.78 μ_B .

The bottom of the conduction band is free-electron-like state with significant amplitudes from atomic O (3s) and Mn (4s) orbitals and it is this state which is responsible for the DFT gap closing in ferromagnetic or spin-disordered phases. For the ferromagnetic phase B3LYP exhibits a gap of 2.4 eV and it is straightforward to check that by decreasing the weight of exact exchange the gap decreases. For example, with 10% of exact exchange in B3LYP the gap lowers to 1.2 eV. The functionals without the exact exchange, such as PW86/PW91/PBE, lead to ferromagnetic metals due to the overlaps with the uppermost valence bands and subsequent rehybridization of states around the Fermi level. This is the "usual" DFT band gap problem which favors smooth and extended states at the expense of the more localized ones which are stabilized by the exact (nonlocal) exchange and correlation effects.

The results presented here therefore provide quite suggestive insights into the problem of a simple one-particle model appropriate for TMOs. In the Mottn-Hubbard picture the origin of the band gap is the large on-site re-

pulsion between the d electrons which basically relates the gap to the two-site $d^n d^n \rightarrow d^{n-1} d^{n+1}$ type of excitation. On the other hand, the charge transfer favors the ionic picture of $M^{n+}O$ with the oxygen p states at the top of the valence band the gap given by the $p \rightarrow d$ excitation energy. Our QMC results quantify that UHF produces qualitatively correct wavefunctions although biased towards the charge transfer limit, especially for excited states. The hybrid B3LYP functional provides more balanced zero-order theory, arguably better and less biased than DFT non-hybrid functionals. This view is supported also by the orbital analysis proposed by Brandow [1, 2], and, in effect, also by introduction of on-site terms which restore some of the Hartree-Fock character. To a certain extent, the hybrid functional alleviates the DFT biases by eliminating part of the self-interaction and by introducing the exchange "pull-down" attraction resulting in lower energies of localized states. Using such orbitals in QMC correlated framework enables us to obtain results which are close to experiment without any additional parameters.

It is tempting to consider the usefulness of a hybrid functional which would be, however, derived from a fundamental theory instead of a fit to a testing set of molecules underlying B3LYP [26]. Although such approach would not fix all the deficiencies of the approximate DFT functionals it could serve, for example, as a cost effective method for providing more appropriate sets of one-particle orbitals for building accurate wavefunctions. In fact, for molecular systems such as TiO and MnO we were able to directly optimize the weight of the exact exchange within a QMC framework. By varying the weight of the exact exchange in the functional and by iterating fixed-node DMC calculations we found the best set of one-particle orbitals which provided the lowest fixed-node energy in DMC [27]; for solids such calculations might be possible in the near future.

In conclusion, we have carried out calculations of the MnO solid in the variational and diffusion Monte Carlo methods. We have evaluated the cohesive and excitation energies which show excellent agreement with experiment. We have pointed out the necessity of using high accuracy Ne-core pseudopotentials for Mn because of semicore 3s and 3p states. The results clearly show a crucial role of both exchange and correlation and their accurate description not only for MnO but obviously for other transition metal oxide systems as well.

This work was supported by the ONR/DARPA grants ONR-N00014-01-1-1062 and ONR-N00014-01-1-0408. Calculations were done as is done on the TITAN-IA 64 cluster at NCSA, at PSC and at PLUTO-P4 cluster in KISTI (Korea Institute of Science and Technology Information). L.M. would like to thank Yoonseok Lee for generously providing his pseudopotentials for testing.

- [2] B. Brandow, *J. Alloys Compounds* 181, 377 (1992).
- [3] J. Zaanen, G. A. Sawatzky, and J. W. Allen, *Phys. Rev. Lett.* 55, 418 (1985).
- [4] J. E. Pask, D. J. Singh, I. I. Mazin, C. S. Hellberg, and J. Kortus, *Phys. Rev. B* 64, 024403 (2001).
- [5] T. Oguchi, K. Terakura, and A. R. Williams, *Phys. Rev. B* 28, 6443 (1983).
- [6] K. Terakura, T. Oguchi, A. R. Williams, and J. Kubler, *Phys. Rev. B* 30, 4734 (1984).
- [7] A. Svane and O. Gunnarsson, *Phys. Rev. Lett.* 65, 1148 (1990).
- [8] Z. Szotek, W. M. Temmerman, and H. Winter, *Phys. Rev. B* 47, R4029 (1993).
- [9] M. R. Norman, *Phys. Rev. B* 44, R1364 (1991).
- [10] V. I. Anisimov, J. Zaanen, and O. K. Andersen, *Phys. Rev. B* 44, 943 (1991).
- [11] J. Hugel and M. Kamal, *Solid State Commun.* 100, 457 (1996).
- [12] M. D. Towler, N. L. Allan, N. M. Harrison, V. R. Saunders, W. C. Mackrodt, and E. Apra, *Phys. Rev. B* 50, 5041 (1994).
- [13] M. W. C. Foulkes, L. Mitas, R. J. Needs, and G. Rajagopal, *Rev. Mod. Phys.* 86, 33 (2001);
- [14] S. Tanaka, *J. Phys. Soc. Jpn.* 62, 2112 (1993); *ibid.* 64, 4270 (1995).
- [15] R. J. Needs and M. D. Towler, in *Proceedings of the 11th International Conference on Recent Progress in Many-Body Theories*, edited by R. F. Bishop, T. Brandes, K. A. G. Gemoth, N. R. Walet, and Y. Xian (World Scientific, Singapore, 2002), p. 434.
- [16] K. E. Schmidt and J. W. Moskowitz, *J. Chem. Phys.* 97, 3382 (1992).
- [17] C. J. Umrigar, K. G. Wilson, and J. W. Wilkins, *Phys. Rev. Lett.* 60, 1719 (1988).
- [18] L. Mitas and R. M. Martin, *Phys. Rev. Lett.* 72, 2438 (1994).
- [19] L. Mitas, E. Shirley, and D. Ceperley, *J. Chem. Phys.* 95, 3467 (1991).
- [20] B. L. Hammond, W. A. Lester, Jr., and P. J. Reynolds, *Monte Carlo Methods in Ab Initio Quantum Chemistry* (World Scientific, Singapore, 1994).
- [21] L. Mitas, *Phys. Rev. A* 49, 4411 (1994).
- [22] M. M. Hurley, L. F. Pacios, P. A. Christiansen, R. B. Ross, and W. C. Ermler, *J. Chem. Phys.* 84, 6840 (1986).
- [23] M. Dohy, U. Wedig, H. Stoll, and H. Preuss, *J. Chem. Phys.* 86, 866 (1987); Yoonseok Lee, private communication.
- [24] T. V. Russo, R. L. Martin, and P. J. Hay, *J. Chem. Phys.* 101, 7729 (1994).
- [25] R. Dovesi, V. R. Saunders, C. Roetti, M. Causa, N. M. Harrison, R. Orlando, and C. M. Zicovich-Wilson, *CRYSTAL98/03 User's Manual* (University of Torino, Torino, 1998/2003).
- [26] A. D. Becke *J. Chem. Phys.* 98, 5648 (1993).
- [27] L. K. Wagner, and L. Mitas, *Chem. Phys. Lett.* 370, 412 (2003).
- [28] D. Ceperley, *Phys. Rev. B* 18, 3126 (1978).
- [29] P. R. C. Kent, R. Q. Hood, A. J. Williamson, R. J. Needs, W. M. C. Foulkes, and G. Rajagopal, *Phys. Rev. B* 59, 1917 (1999).